*17th World Conference on Earthquake Engineering, 17WCEE*
*Sendai, Japan - September 13th to 18th 2020*

# CYCLIC TESTS OF GLULAM FRAMES WITH BUCKLING RESTRAINED BRACES

Wenchen Dong[(1)], Minghao Li[(2)], Chin-Long Lee[(3)];Gregory MacRae[(4)], Anthony Abu[(5)]

[(1)] *PhD candidate, University of Canterbury, wenchen.dong@pg.canterbury.ac.nz*
[(2)] *Senior Lecturer, University of Canterbury, minghao.li@canterbury.ac.nz*
[(3)] *Senior Lecturer, University of Canterbury, chin-long.lee@canterbury.ac.nz*
[(4)] *Associate Professor, University of Canterbury, gregory.macrae@canterbury.ac.nz*
[(5)] *Associate Professor, University of Canterbury, anthony.abu@canterbury.ac.nz*

## *Abstract*

In this study, an attempt was made to integrate BRBs to glulam frames to provide strength, stiffness, ductility and energy dissipation. Two 8 m wide, 3.6 m high full-scale BRB glulam frame (BRBGF) specimens were designed using capacity design approach and tested under cyclic loading. The BRBs were designed as ductile elements in the hybrid system to dissipate energy under seismic loading and connections and glulam members were designed to remain elastic. The BRBs were connected to the glulam frames by pins and steel gusset plates. Dowelled connections were used in one specimen to connect the glulam members while screwed connections were used in the other. The dowelled connections used Φ12 mm dowels and two 20 mm thick inserted steel plates; the screwed connections used Φ11x300 mm inclined self-tapping screws and two 12 mm thick steel side plates. Both specimens were tested to 1.5% drift ratio. The tests showed that specimens carried high lateral load and achieved a minimum ductility factor of 3.0 according to EN 12512. The connections were well protected with limited damage and negligible moment resisting capacity. Both connections were able to engage the BRBs efficiently and resist the anticipated inelastic demand. The integration of BRBs into glulam frames improved the load carrying capacity, ductility and energy dissipation compared to conventionally timber brace frame (TBF).

*Keywords: buckling restrained braces (BRBs); glulam; dowelled connection; screwed connection*

 



## 1. Introduction

With more availability of high performance engineered timber products, there are increasing interests in building multi-storey engineered timber buildings around the world. Braced frames are one of the popular lateral force resisting systems (LFRS) in heavy timber buildings. In conventionally braced heavy timber frames under seismic loading, energy dissipation primarily relies on the connections between the timber braces and main frame. However, any severe damage to timber members and connections after major earthquakes is difficult to repair. Steel braces may improve system ductility as they can yield and dissipate energy. However, steel concentrically braced frames (CBF) may still show limited ductility and overall poor seismic performance due to the buckling of braces [1]. Buckling restrained braces (BRBs) can restrain the buckling of steel braces in compression and achieve similar behaviour under tension and compression. Past BRB component tests and BRB steel frame tests [2] demonstrated high ductility and predictable seismic behaviour. Therefore, it is possible to improve seismic performance of heavy timber frames by integrating BRBs to form a hybrid LFRS.

In this study, an attempt was made to integrate BRBs to glulam frames to provide strength, stiffness, ductility and energy dissipation. Two full-scale BRB glulam frame (BRBGF) specimens were designed using capacity design approach and tested under cyclic loading. Previous research showed that connections made of dowels [3-5] and inclined self-tapping screws [6, 7] could achieve high strength and stiffness. Therefore, these two types of connections were used to form the critical BRB-glulam interface connections as well as the glulam beam-column connections. The objective is to assess the strength, stiffness, ductility and energy dissipation of this hybrid system.

## 2. Specimen design

### 2.1 Prototype building

A six-storey glulam office building located in Christchurch, New Zealand, was used as a prototype building to design the BRBGF specimens as shown in Fig. 1. The seismic demand calculation followed the equivalent static method in New Zealand standards NZS 1170.5 [8] and the load taken by each frame is shown in Fig.1 as well. The BRBGF on the second storey was chosen as the design specimens. Two BRBGF specimens (S-D and S-S) were designed and Fig. 2 shows the specimen setup. Both specimens were 8 m wide and 3.6 m high. The two specimens were identical except for the use of different connection details. S-D used dowels and inserted steel plates (referred as the dowelled connections) and S-S used inclined self-tapping screws and steel side plates (referred as the screwed connections).

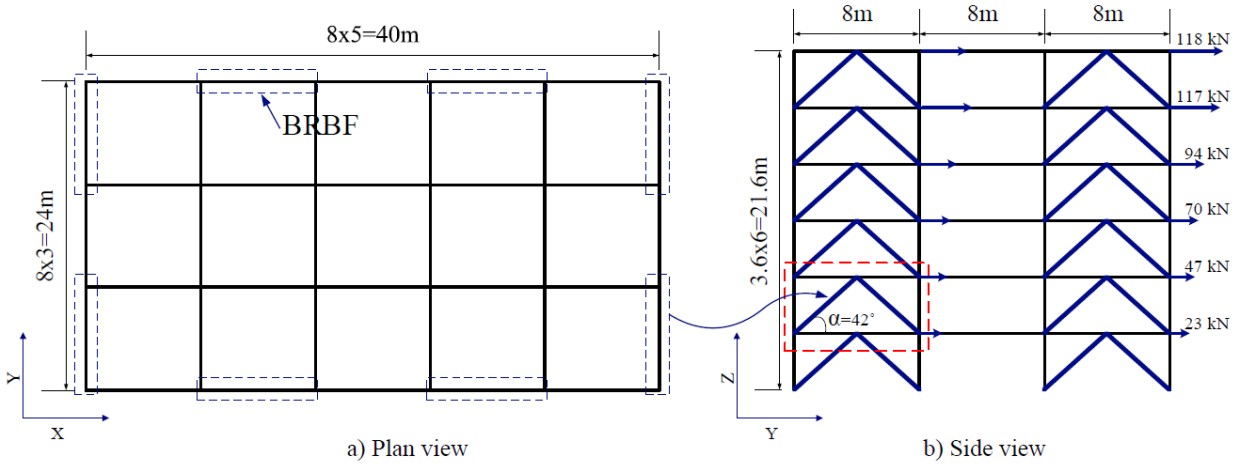


Fig. 1 –Prototype Building



 



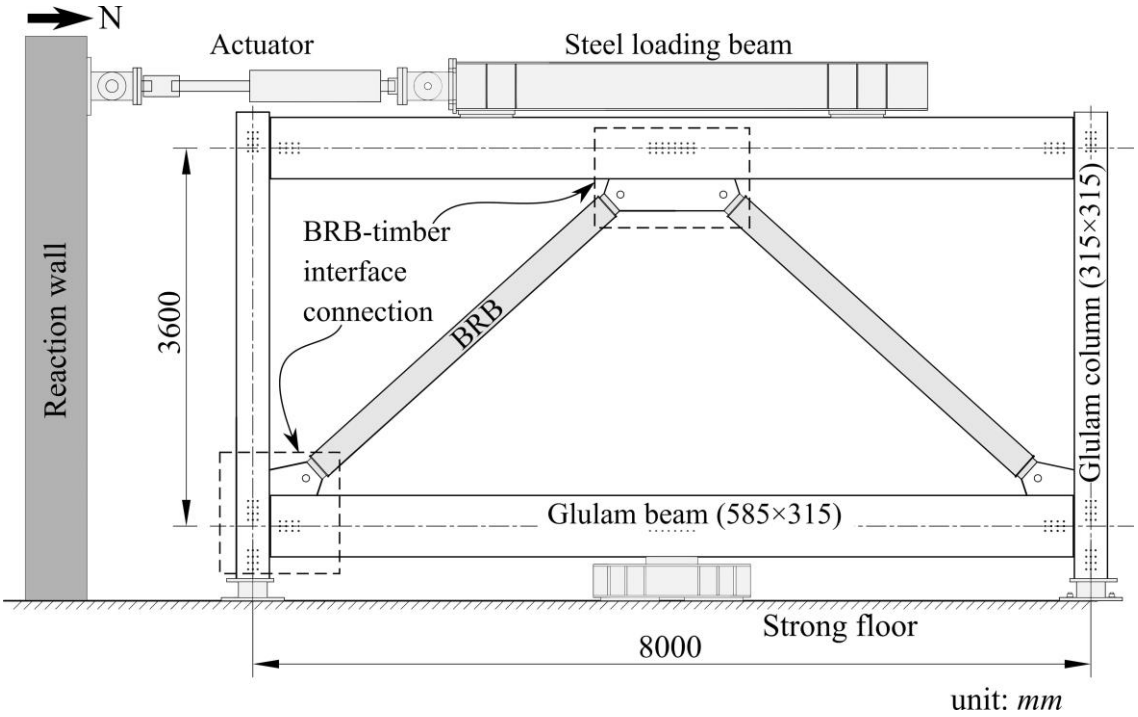


Fig. 2 – Specimen setup

## 2.2 Capacity design

Following the capacity design approach, BRBs in this hybrid system are assumed as ductile elements and all glulam members and connections are non-ductile elements and protected from significant damage or repair under major earthquakes. According to the specification in American steel code AISC 341-16 [9] for steel BRB frame, Eq. (1) was used for the glulam members and connections design.

$$R_{d,brittle} \geq R_y \omega \beta R_{k,BRB} \quad (1)$$

where, $R_{d,brittle}$ is the capacity of non-ductile/brittle members; $R_y$ (=1.15) is the material overstrength factor according to AISC 341-16; ω is the BRB strain hardening adjustment factor; β is the BRB compression strength adjustment factor; $R_{k,BRB}$ ($=f_{ys}A_s$) is the characteristic yield capacity of BRB and $A_s$ is the area of the steel core.

## 2.3 BRB member design

The ultimate limit state (ULS) seismic load demand for the test specimens was 447 kN which caused a load demand of 301 kN for each BRBs in term of the angle α in Fig. 1. Commercial BRB products were used in this study with predicted yield strength $F_{y,pred}$ of 303 kN and ωβ=1.5. The steel core was a Grade Q235 [10] flat steel plate with a cross section of 70 mm × 16 mm, and steel casing was a 250 mm × 250 mm × 6 mm Grade Q235 square tube. C30 concrete [11] was used to fill the space between the steel core and the steel casing. Φ70 mm pin connections were used to connect BRBs with the steel gusset plates. All gusset plates were designed according to NZS3404 [12] and AISC 360-16 [13].

## 2.4 Glulam member and connection design

GL10 grade Radiata Pine glulam [14] with characteristic density of 434 kg/m$^3$ was used as beams and columns. Since BRBs do not carry gravity loads after yielding, the glulam beams were designed with a full span of 8 m. The beam and column cross sections were 585 mm × 315 mm and 315 mm × 315 mm, respectively considering all possible load combinations in the prototype building. There was also a 10 mm gap between the glulam beam and column to allow for the joint rotation without causing significant crushing on the column.



 



In S-D, the dowelled connections consisted of Φ12 mm Grade 300 [12] steel dowels and 20 mm thick Grade 300 steel plates as shown in Fig. 3a. The beam-column connections had 12 dowels for either beam or column side and the middle span connection had 24 dowels. Each connection had two internal steel plates as gusset plates that had Φ13 mm predrilled holes for the dowels. The glulam members had two 22 mm wide slots with a spacing of 125 mm and Φ12 mm holes. The design strength of the dowelled connections was calculated using the model proposed by Fan [15] and European Yield Models in Eurocode 5 [16] considering the effective number $n_{ef}$ of dowels in each row. Dowel groups in all connections aligned along the glulam member axes to reduce the moment caused by eccentricity.

In S-S, the screwed connections consisted of Rothoblaas Φ11 × 300 mm VGS screws, VGU washers and 12 mm thick Grade 350 [12] steel plates, as shown in Fig. 3b. The beam-column connections had 32 screws on column side and 34 screws on beam side and the middle span connection had 64 screws. Each connection had two steel side plates as gusset plates. The washers were used to accommodate the 45˚ inclined screw installation. Slotted holes for the washers were laser cut on the gusset plates. The geometry of the washers actually limited the gusset plate thickness to 12 mm. Stiffeners were welded to the gusset plates to avoid out-of-plane buckling under compression loads. All screws were considered as tension-only screws (black screws under the force shown in Fig. 3b) as the length of slotted holes were 4 mm longer than the length of the washers. The design strength of the screwed connections was the horizontal component, $R_{sx}$, of the axial strength $R_s$, which was calculated according to Eurocode 5 as axially loaded screws. No friction contribution was accounted and the effective number of screws, $n_{ef}$ was chosen to be 0.9n (n is the total number of screws in tension) based on the tests by Krenn [6].

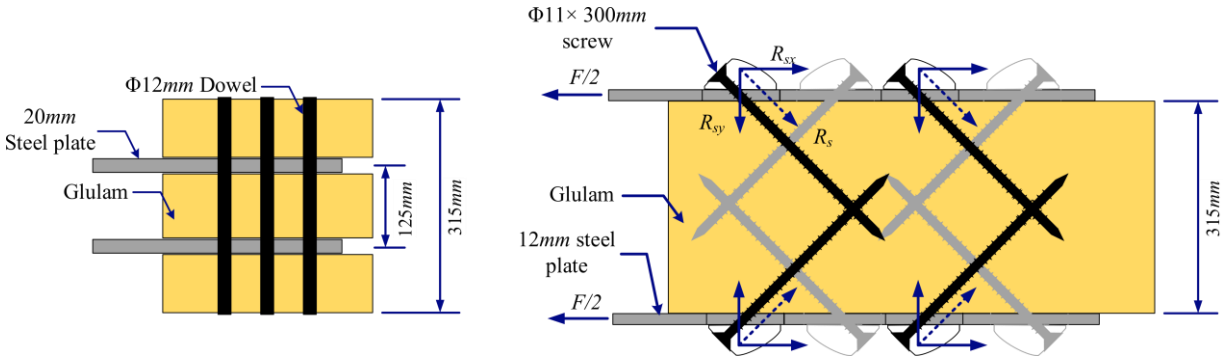


(a) Dowelled connection (b) Screwed connection

Fig. 3 – Connection details

## 3. Test programme

### 3.1 Test matrix and loading protocol

The tests had two phases: frame tests and BRB component tests. Fig. 4 shows the frame specimens in testing. The column bases and the mid-span shear connection of the bottom glulam beam were anchored to the strong floor by steel brackets and dowelled connections. The top glulam beam was connected to a steel loading beam that was also connected to an 800 kN actuator mounted on the reaction wall. The out-of-plane restraints of the specimens were provided by two actuators at the positions of the columns. The BRB component tests were used to check the BRB design parameters such as ω and β, ensuring that they were consistent with the specification. Three BRB component tests were conducted under uniaxial cyclic loading as shown in Fig. 5. Two BRBs (BRB-D and BRB-S) were taken from S-D and S-S after the frame tests. One BRB (BRB-U) was unused but manufactured in the same batch as the BRBs installed in the frames.



 



Table 1 lists the test matrix and objectives. The drift ratio illustrates the maximum drift ratio achieved in each test. The frame tests and BRB component tests followed the loading protocol in ISO 16670 [17] and AISC 341-16, respectively. The BRBF tests were finished at 1.5% drift ratio because the loading capacity of the actuator was reached. Rest of the tests were loaded to design drift ratio (2%).

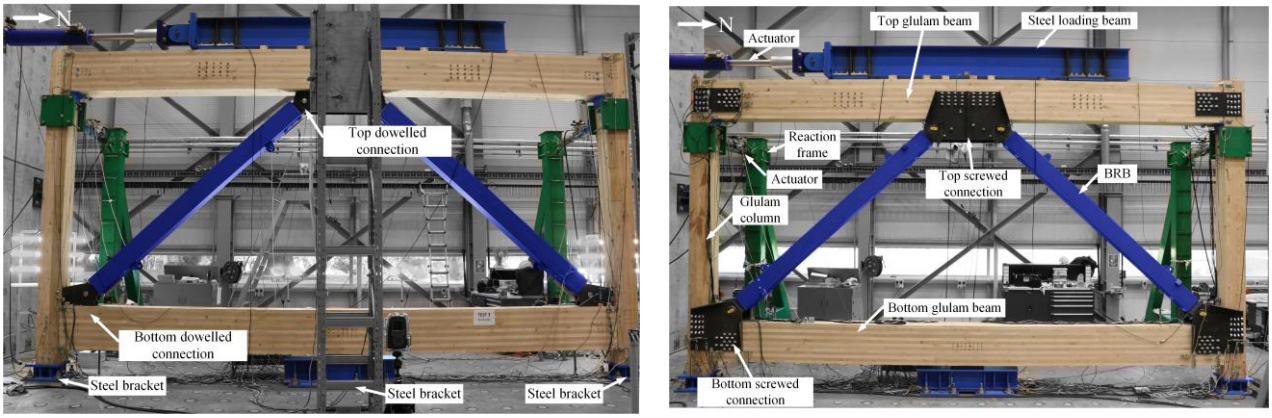


(a) S-D with dowelled connections (b) S-S with screwed connections

Fig. 4 – Frame test specimens

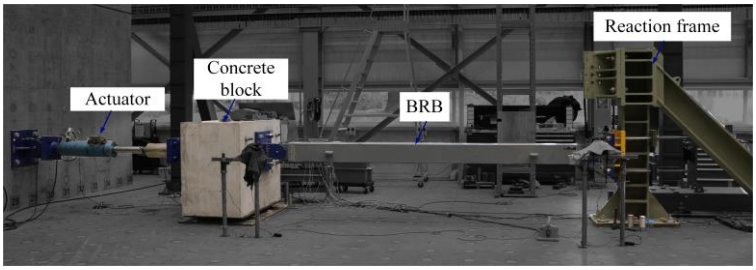


Fig. 5 – BRB component tests

Table 1 – Test matrix

| **Test phase** | **Specimen name** | **Test No.** | **Objective** | **Drift ratio** |
|---|---|---|---|---|
| I: frame tests | S-D | T1: BRBGF cyclic test | Evaluate ULS | 1.5% |
| | | T2: bare frame test | Evaluate the bare frame's deformation capacity | 2.0% |
| | S-S | T3: BRBGF cyclic test | Evaluate ULS | 1.5% |
| | | T4: bare frame test | Evaluate the bare frame's deformation capacity | 2.0% |
| II: BRB component tests | BRB-D | T5:cyclic test | Evaluate the BRB residual performance | 2.0%* |



 



| | | | | |
|---|---|---|---|---|
| | BRB-S | T6: cyclic test | Evaluate the BRB residual performance | |
| | BRB-U | T7: cyclic test | Evaluate the BRB property | |

* BRBs were loaded to the displacement they would achieve when the BRBGF was loaded to the drift ratio

### 3.2 Instrumentation

Load cells were used to measure the actuator force; inclinometers were used to measure the connection rotation; string potentiometers were used to measure the frame lateral displacement and out-of-plane movement; linear-motion potentiometers (LPs) were used on both side of BRBs to measure BRBs' tensile and compressive deformation as shown in Fig. 6.

Fig. 6 – The linear-motion potentiometer for measuring BRB deformation

## 4. Test results

### 4.1 BRBGF specimen response

Residual deformation in the BRBs (as shown in Fig. 7) and the hybrid frames was observed in both specimens loaded up to 1.5% drift ratio until the actuator reached the loading capacity. In S-D, a small number of dowels experienced minor bending deformation, as shown in Fig. 8. In S-S, slight bending deformation at the edge of the gusset plates was observed in the top connection as shown in Fig. 9 when the lateral load was over the design value. Screws were removed from the screwed connections and no visible damage was observed.

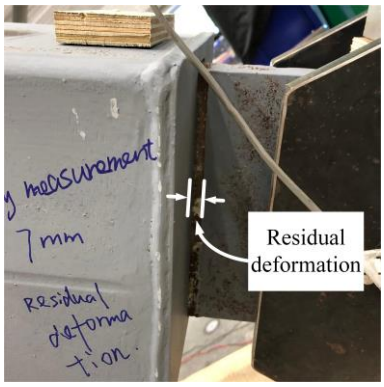


Fig. 7 – BRB residual deformation in S-D specimen

Fig. 8 – Dowels' bending in S-D specimen

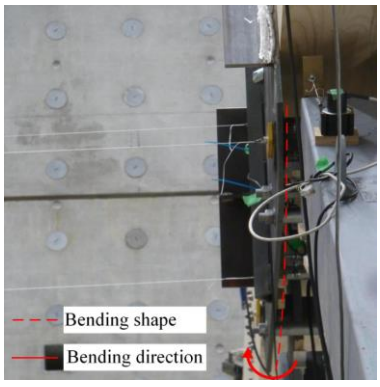


Fig. 9 – Top gusset plate bending in S-S specimen



 



## 4.2 Load-drift hysteresis curves of BRBGF specimens

For tests T1 and T3, the frame hysteresis curves and backbone curves are shown in Fig. 10. The drift was the inter-storey drift after removing the slips of the foundation. The full hysteresis curves displayed similar performance with BRB steel frames as the yielding of the BRBs provided the energy dissipation and governed the BRBGF specimen behaviour. It also indicated that limited energy dissipation occurred in the glulam connections as the hysteresis curves of timber connections under cyclic loading typically had the pinching effect, which was consistent with the observed specimen response of connections during tests.

Fig. 10a shows that S-D experienced three stages: initial slip stage, elastic stage and post-yield stage. First, the initial stiffness was low when the drift was within ±4.5 mm. The initial slip was primarily attributable to three factors: (1) the holes on BRBs for the pinned connections were manufactured by plasma cutting and were up to 2 mm oversized; (2) the holes in the gusset plates for the dowels were 1 mm oversized for installation convenience; (3) the stiffness of the surface layers of the dowel holes was lower than those of the surrounding bulk wood [18]. After the initial slip stage, BRBs were fully engaged in carrying the loads and the system became very stiff until BRBs yielded. The stiffness of S-D decreased gradually after the BRBs yielded. The maximum residual drift ratio was 0.89% (32.1mm).

Fig. 10b shows that S-S had similar performance to S-D. The main difference was that S-S had less initial slip, which was within ±2.0 mm. It was because the inclined screws engaged in the axial direction were much stiffer compared with laterally loaded dowels with similar diameters [6]. However, the unloading process shows that the slip gradually increased at around zero load. This was primarily due to the loosening of the inclined screw washers under cyclic loading. The rotation of joints caused lateral movement of screws, and the oversized slotted holes allowed the washers to slip laterally and axially. As a result, some washers became loose and gaps were observed between washers and screw heads during testing as shown in Fig. 11. These screws were not in tension again until the washers contacted the gusset plates. The maximum residual drift ratio was 0.88% (31.5 mm).

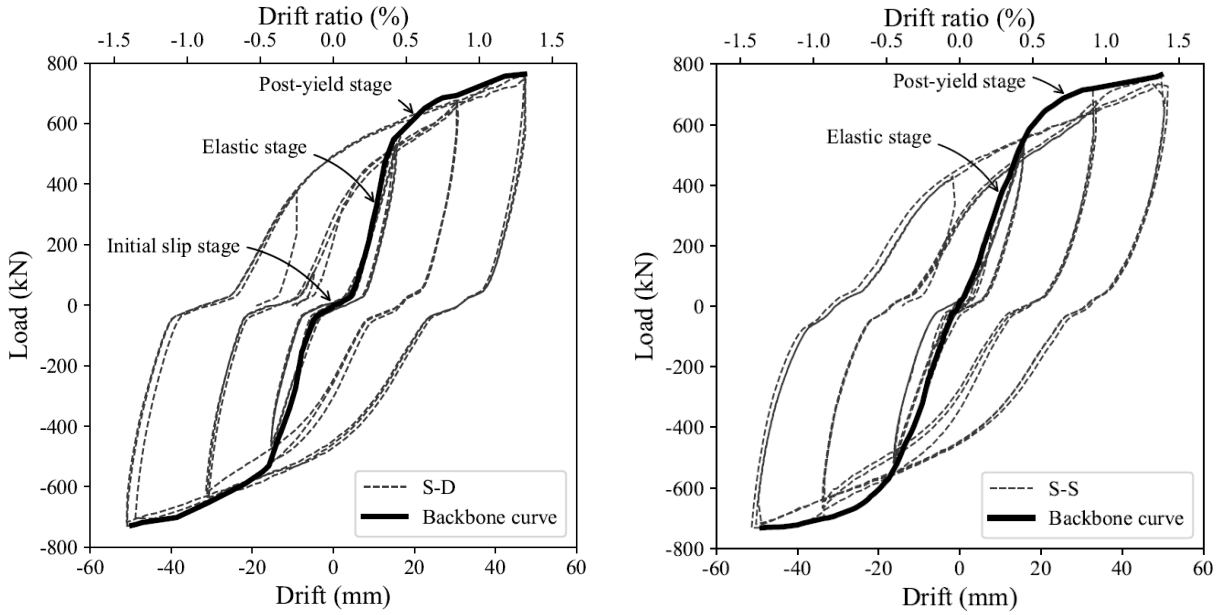


(a) S-D with dowelled connection (b) S-S with screwed connection

Fig. 10 – Hysteresis curves and backbone curves



 



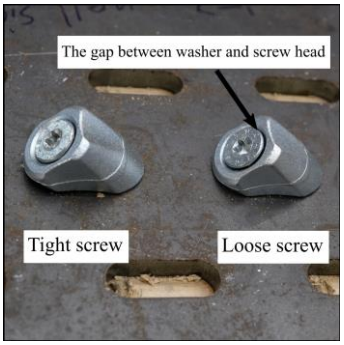


Fig. 11 – The loose screws caused by rotation of the joints

Following the test standard EN12512 [19], the lateral properties of S-D and S-S were derived by the load-drift backbone curves, as listed in Table 2. The maximum strength of both specimens exceeded 750 kN. In the past full-scale tests about traditional timber brace frame (TGF) [20, 21], the ultimate strength was all lower than 200 kN with smaller cross section members primarily designed for low-rise buildings. S-D and S-S showed much higher strength capacity that provided possibility of application in mid-rise buildings. The stiffness at elastic stage and post-yield stage were defined as elastic stiffness $k_1$ and plastic stiffness $k_2$. In addition, the stiffness degradation of backbone curves was derived according to the variation of their tangent stiffness and is shown in Fig. 12. S-D had low initial stiffness but reached a higher stiffness than S-S when the BRBs were engaged. This indicated that the dowelled connections were very stiff after overcoming the initial slip.

Table 2 – Strength, stiffness and ductility properties of two frame specimens

| **Property** | **S-D** | | | **S-S** | | |
|---|---|---|---|---|---|---|
| | **Positive** | **Negative** | **Mean** | **Positive** | **Negative** | **Mean** |
| Maximum strength $F_{max}$ (kN) | 763.5 | 729.9 | 746.7 | 764.4 | 731.8 | 748.1 |
| Maximum drift $\delta_{max}$ (mm) and drift ratio (%) | 47.4 (1.3) | 51.0 (1.4) | 49.2 (1.4) | 51.3 (1.4) | 51.3 (1.4) | 51.3 (1.4) |
| Yield Force $F_y$ (kN) | 595.6 | 539.6 | 567.6 | 626.5 | 593.1 | 609.8 |
| Yield drift $\delta_y$ (mm) and drift ratio (%) in brackets | 15.5 (0.4) | 14.7 (0.4) | 15.1 (0.4) | 16.9 (0.5) | 16.2 (0.5) | 16.6 (0.5) |
| Elastic stiffness $k_1$ (kN/mm) | 55.2 | 53.2 | 54.2 | 38.7 | 40.4 | 39.5 |
| Plastic stiffness $k_2$ (kN/mm) | 6.0 | 5.6 | 5.8 | 4.5 | 5.1 | 4.8 |
| Initial slip $\delta_s$ (mm) | 4.7 | 4.5 | 4.6 | 0.7 | 1.6 | 1.2 |
| Ductility factor μ (CEN) | 3.1 | 3.5 | 3.3 | 3.0 | 3.1 | 3.1 |
| Ductility factor μ (EEEP) | 2.1 | 2.4 | 2.3 | 2.6 | 2.9 | 2.8 |

The ductility factor μ is normally defined by Eq. (2), which is the ratio between the ultimate drift $\delta_u$ and the yield drift $\delta_y$. $\delta_u$ is normally defined as the drift at which the load drops to 80% of the peak load. In the BRBGF testing, since no obvious failure or load decrease were observed, $\delta_u$ was assumed as maximum



 



drift at the peak load $\delta_{max}$. The CEN method in EN12512 was used to calculate $\delta_y$ since it provided a reasonable value for system with an elevated initial stiffness [22]. The TBF tests with similar brace layout [20] presented μ ranging from 1.0 to 1.2 based on EEEP method [23]. In order to compare with them, μ of BRBGF based on EEEP method is also listed in Table 2, which ranged from 2.3 to 2.8. The ductility of BRBGF was double compared to TBF. It should be noted that the μ of BRBGF is the minimum value as the post-peak ultimate displacement was not reached.

$$\mu = \delta_u / \delta_y \quad (2)$$

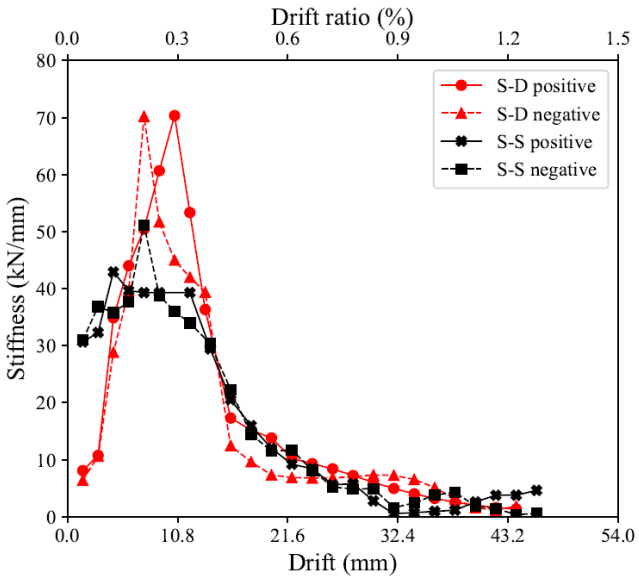


Fig. 12 – Stiffness degradation of the backbone curves

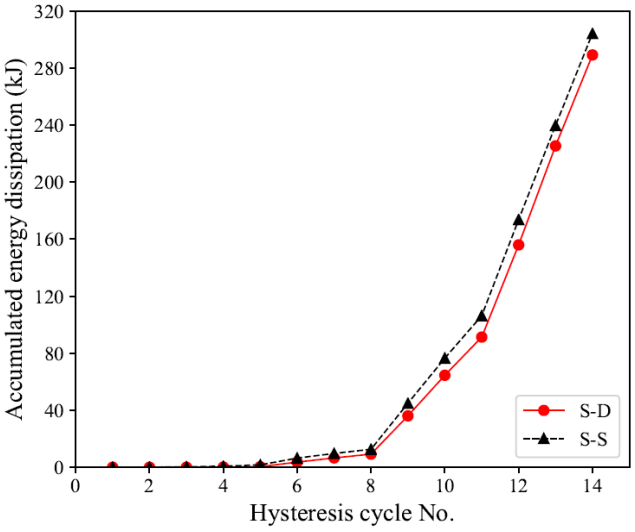


Fig. 13 – Energy dissipation capacity of two specimens

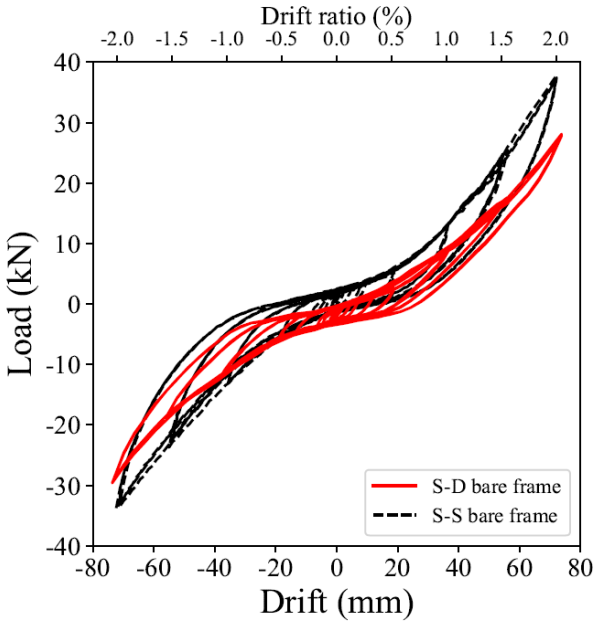


Fig. 14 – Bare frame hysteresis curves

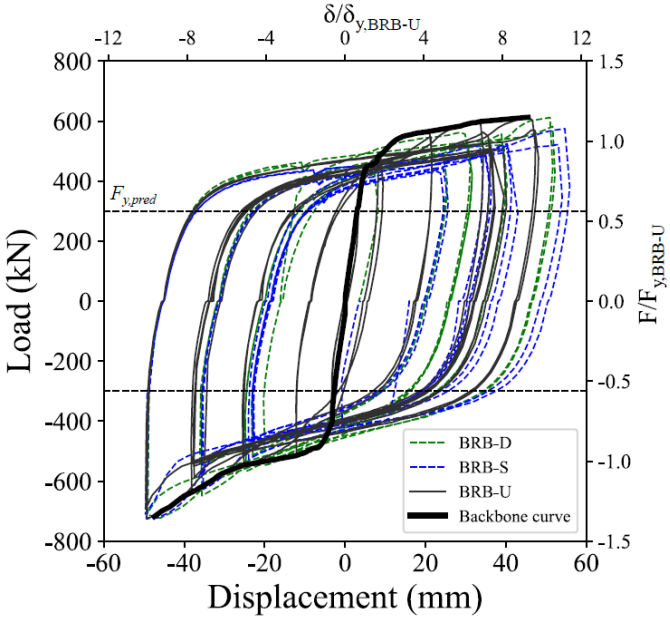


Fig. 15 – BRB hysteresis curves



 



Fig. 13 shows energy dissipation of S-D and S-S over the loading cycles. S-D and S-S dissipated 289 kJ and 304 kJ in 14 cycles, respectively. However, the TBF test with peak load 129.5 kN and ultimate displacement 63.6 mm (2.5% drift ratio) could only dissipated less than 25 kJ energy in 28 cycles until brace connection failure [20]. In terms of the limited energy that brace connections can dissipate, it is expected that the BRBF have much higher energy dissipation capacity compared to TBF.

In test T2 and T4, BRBs in S-D and S-S were removed and two bare frames were tested to 2.0% drift ratio. The hysteresis curves are shown in Fig. 14. It was found that the bare frames' contribution to the total lateral load capacity of the hybrid system was less than 5% at 1.5% drift ratio. Therefore, both connections had negligible moment resisting capacity and could resist at least 2.0% drift ratio inelastic demand.

### 4.3 BRB component tests

Fig. 15 shows the hysteresis curves of three BRBs and the backbone curve of BRB-U. Three BRBs had similar hysteresis curves, thus the performance of this batch of BRBs was consistent and BRB-U could stand for the performance of those used in the frame tests. The accumulated ductility factor of BRB-U was 302, meeting the minimum requirement 200 in AISC 341-16. Fig. 15 also shows the ratios of BRB displacement $\delta$ to yield displacement $\delta_{y,\,BRB\text{-}U}$, BRB load F to actual yield load $F_{y,\,BRB\text{-}U}$ and BRB's predicted yield force $F_{y,pred}$ to calculate $\omega$, $\beta$ and $R_y$. The average $\delta_y$, $\omega$, $\beta$, $R_y$ from the positive and negative backbone curves were 4.9 mm, 1.26, 1.18 and 2.06, respectively. The $\omega\beta$ =1.49 matched with the supplier's information but the $R_y$ was significantly higher than the assumed value 1.15. To find the reason for the significantly higher $R_y$, BRB-U was taken apart and the steel core was extracted and cut as steel coupons to check the steel core property. $R_y$ from steel coupon tests was 1.25, which was slightly higher than 1.15 but much lower than 2.06. It was found that the unbonding layers stuck to the steel core and concrete grout tightly. The improper unbounding could cause high friction between steel core and concrete grout. In term of that, it was likely that the high friction and Poisson effect caused the extra overstrength. As suggested by MacRae et al. [24], BRB quality control is essential during capacity design to ensure BRB's performance is consistent with the specification.

## 5. Conclusions

The cyclic performance of two full-scale BRB glulam frames were experimentally studied. Capacity design approach was used to design the hybrid system. Dowelled and screwed connections were used to connect glulam frames with BRBs via steel gusset plates. The primary findings are listed as follows:

- The hybrid frames had load-carrying capacity of over 750kN, much higher than those in the past timber brace frame (TBF) tests. Connections were well protected with limited damage. The capacity design proved to work well for the hybrid frame system.
- Under cyclic loading, the hybrid frames had full hysteresis curves and dissipated 289 kJ and 304 kJ energy in 14 loading cycles, respectively. The minimum ductility factor exceeded 3.0 according to EN12512. The ductility and energy dissipation were improved significantly compared to TBF.
- BRBs, as the ductile members in capacity design, requires strict quality control or sample test during timber connection design to make sure that BRBs' performance is consistent with their specification.

## 6. Acknowledgements

The authors would like to thank the Natural Hazards Research Platform in New Zealand, QuakeCore, University of Canterbury, Shanghai Research Institute of Materials, Timber Connect Limited and New Zealand Timber Design Society for partially sponsoring the project. The authors appreciate the technical support provided by Prof. Roger Nokes, technicians Russell McConchie, Alan Thirlwell, Michael Weaver and Peter Coursey from University of Canterbury.



 



## 7. References

[1] S. Hussain, P. Van Benschoten, M. Al Satari, and S. Lin, "Buckling Restrained Braced Frame (BRBF) Structures: Analysis, Design and Approvals Issues," in *The 75th SEAOC Annual Convention, September 13-16*, 2006.

[2] C. Uang, M. Nakashima, and K. Tsai, "Research and application of buckling-restrained braced frames," *Int. J. Steel Struct.*, vol. 4, no. 4, pp. 301–313, 2004.

[3] L. M. Ottenhaus, M. Li, T. Smith, and P. Quenneville, "Overstrength of dowelled clt connections under monotonic and cyclic loading," *Bull. Earthq. Eng.*, vol. 16, no. 2, pp. 753–773, 2018.

[4] L. M. Ottenhaus, M. Li, T. Smith, and P. Quenneville, "Mode Cross-Over and Ductility of Dowelled LVL and CLT Connections under Monotonic and Cyclic Loading," ASCE *J. Struct. Eng.*, vol. 144, no. 7, pp. 1–10, 2018.

[5] L. M. Ottenhaus, M. Li, and T. Smith, "Structural performance of large-scale dowelled CLT connections under monotonic and cyclic loading," *Eng. Struct.*, vol. 176, no. September, pp. 41–48, 2018.

[6] H. Krenn and G. Schickhofer, "Joints with inclined Screws and Steel Plates as outer Members," in *Proceedings of the international council for research and innovation in building and construction, Working commission W18 – timber structures, Meeting 42*, 2009.

[7] M. Closen, "Self-Tapping Screw Assemblies Under Monotonic Loading," The University of British Columbia, 2012.

[8] Australia and New Zealand Standards, *NZS1170.5: Structural design actions - Part 5: Earthquake actions-New Zealand*. Wellington, New Zealand, 2004.

[9] American Institute of Steel Construction (AISC), *Seismic provisions for structural steel buildings. ANSI/AISC 341-16*. Chicago, IL, 2016.

[10] Chinese Global Standards, *GB50017-2017: Code for Design of Steel Structures*. Beijing, China: China Architecture & Building Press Beijing, China, 2017.

[11] Chinese Global Standards, *GB50010-2010: Code for design of concrete structures*. Beijing, China: China Architecture & Building Press Beijing, China, 2010.

[12] New Zealand Standards, *NZS 3404: Part 1:1997 - Steel Structure Standard*. Wellington, New Zealand: New Zealand Standards, 1997.

[13] American Institute of Steel Construction (AISC), *ANSI / AISC 360-16, Specification for Structural Steel Buildings*. 2016.

[14] New Zealand Standards, "NZS3603:1993 Timber structures standard," no. 1. Standards New Zealand, Wellington, New Zealand, 1993.

[15] X. Fan, S. Zhang, and W. Qu, "Load-carrying behaviour of dowel-type timber connections with multiple slotted-in steel plates," *Appl. Mech. Mater.*, vol. 94–96, pp. 43–47, 2011.

[16] British Standard Institution (BSI), "Eurocode 5: design of timber structures—Part 1-1: General—Common rules and rules for buildings." BSI, London, 2004.

[17] International Organization for Standardization (ISO), "Timber structures—Joints made with mechanical fasteners—Quasi-static reversed-cyclic test method, ISO16670." ISO, London, 2003.

[18] M. Dorn, "Investigations on the Serviceability Limit State of Dowel-Type Timber Connections," PhD dissertation, Vienna University of Technology, 2012.

[19] British Standard Institution (BSI), "BS EN 12512:2001: Timber structures. Test methods. Cyclic testing of joints made with mechanical fasteners." British Standards Institute, London, 2002.

[20] H. Xiong, Y. Liu, Y. Yao, and B. Li, "Experimental study on the lateral resistance of reinforced glued-laminated timber post and beam structures," J. Asian Archit. Build. Eng., vol. 16, no. 2, pp. 379–385, 2017.

[21] M. Popovski, H. G. L. Prion, and E. Karacabeyli, "Shake table tests on single-storey braced timber frames," Can. J. Civ. Eng., vol. 30, no. 6, pp. 1089–1100, 2003.



 




[22] W. Muñoz, A. Salenikovich, M. Mohammad, and P. Quenneville, Determination of yield point and ductility of timber assemblies: In search for a harmonised approach. 10th World Conference on Timber Engineering 2008, 2, 1064–1071, 2008.

[23] American Society for Testing and Materials, Standard Test Methods for Cyclic ( Reversed ) Load Test for Shear Resistance of Vertical Elements of the Lateral Force Resisting Systems forBuildings. E2126, 11(Reapproved 2018), 1–15, 2011.

[24] G. A. Macrae and G. C. Clifton, "Research on Seismic Performance of Steel Structures," Steel Innov. 2015 Conf., no. September, pp. 3–4, 2015.



 